Lattice-Symmetry-Assisted Second-Order Topological Superconductors and Majorana Patterns

Xiao-Hong Pan,[1,2] Kai-Jie Yang,[1,3] Li Chen,[1,2] Gang Xu,[2,1] Chao-Xing Liu,[3] and Xin Liu[1,2,*]
[1]School of Physics, Huazhong University of Science and Technology, Wuhan, Hubei 430074, China
[2]Wuhan National High Magnetic Field Center, Huazhong University of Science and Technology, Wuhan, Hubei 430074, China
[3]Department of Physics, the Pennsylvania State University, University Park, Pennsylvania 16802, USA

(Received 21 January 2019; published 10 October 2019)

We propose a realization of the lattice-symmetry-assisted second-order topological superconductors with corner Majorana zero modes (MZM) based on two-dimensional topological insulators (2DTI). The lattice symmetry can naturally lead to the anisotropic coupling of edge states along different directions to the in-plane magnetic field and conventional s-wave pairings, thus leading to a single MZM located at the corners for various lattice patterns. In particular, we focus on the 2DTI with D_{3d} lattice symmetry and found different types of gap opening for the edge states along the armchair and zigzag edges in a broad range of parameters. As a consequence, a single MZM exists at the corner between the zigzag and armchair edges, and is robust against weakly broken lattice symmetry. We propose to realize such corner MZMs in a variety of polygon patterns, such as triangles and quadrilaterals. We further show their potentials in building the Majorana network through constructing the Majorana Y junction under an in-plane magnetic field.

DOI: 10.1103/PhysRevLett.123.156801

Introduction.—Majorana zero modes (MZMs) in topological superconductors (TSCs) have been extensively studied recently [1–21] because of their non-Abelian braiding statistics [1,22,23] and the potential application in topological quantum computation (TQC). Although the great experimental progress in several condensed matter platforms have lead to the observance of a zero bias conductance peak [5,6,18–20] and 4π Josephson effect [7,16,17,24,25], the deterministic evidence of the non-Abelian braiding statistics is still lacking for MZMs, which is essential for TQC. As the experimentally measurable braiding requires at least four MZMs, it is worthwhile to search for new platforms that allow for the appearance of multiple MZMs. The recent studies of the second-order topological states [26–60] have brought new insights in realizing MZMs. In contrast to conventional n-dimensional topological insulators (TIs), the second-order TIs are characterized by topological protected gapless states in n-2 dimensions. Particular for the two-dimensional second order TSCs [38,44,50–52,56,58], the current proposals [50,52,58] are based on s-, $s_{\pm}$-, or d-wave superconductors and, at each corner, they support a pair of MZMs protected by additional time-reversal or mirror symmetry. Since it is difficult to reveal non-Abelian statistics when MZMs are paired, it is thus more desirable to look for second-order TSC with a single MZM at each corner. As there is no need of additional symmetry to protect a local single MZM, such a system is also more robust against the environmental perturbation.

In this Letter, we demonstrate the realization of a single MZM at certain corners of the 2DTIs within a honeycomb lattice in proximity to the conventional s-wave superconductor under an in-plane magnetic field. These 2DTIs include the bismuthene and silicene, whose topological bands around a Fermi surface are dominated by $\{p_x, p_y\}$ and p_z orbitals, respectively. Even in the quite general case for these different 2DTI models, we found that the helical edge states at the armchair edge still remain almost gapless while those at the zigzag edge are fully gapped. The anisotropic coupling of the edge states to the uniform in-plane magnetic field is due to the fact that the mirror symmetry at the degenerate point of the edge states is preserved along the armchair edge but broken along the zigzag edge. With further applying the uniform s-wave superconducting pairing term, a superconducting gap is opened at the armchair edge while a magnetic gap occurs at the zigzag edge in a large parameter regime. As a result, we demonstrate a single MZM existing at the corner between the armchair and zigzag edges. We further identify two types of triangular patterns in the honeycomb lattices [Figs. 1(a) and 1(b)], each of which supports two MZMs located separately at two corners of the triangle and is thus equivalent to a Majorana nanowire [1–4]. We thus refer to these patterns as Majorana triangles. More importantly, as the existence of MZMs in these patterns is independent of the in-plane magnetic field directions, we show that the Majorana triangles can have six orientations [Figs. 1(a) and 1(b)] and thus can construct a more complex Majorana network such as a Y junction under an uniform in-plane magnetic field [Fig. 1(c)]. Note that no additional symmetry other than the intrinsic particle-hole symmetry is required, and these MZMs are robust against the terms that

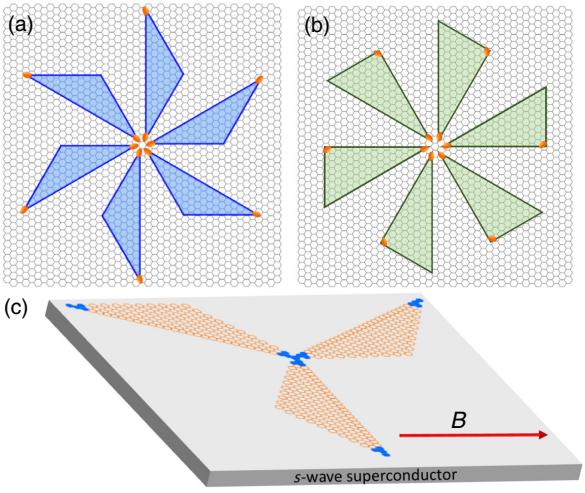

FIG. 1. (a) The Majorana isosceles triangle in six orientations. (b) The Majorana right triangles in six orientations. Each Majorana triangle is equivalent with a Majorana nanowire along the six orientations. (c) Y junction made from three Majorana isosceles triangles.

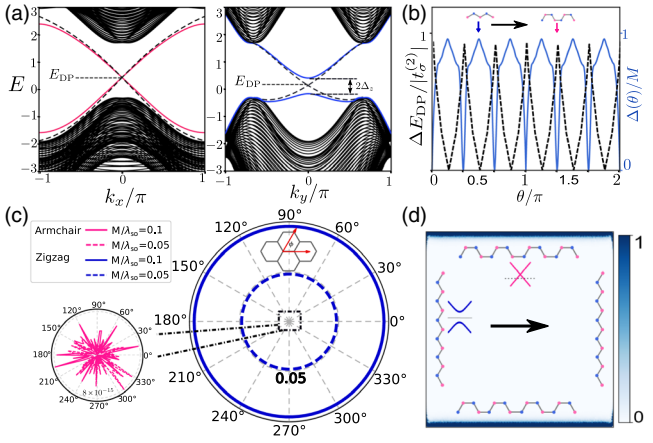

FIG. 2. (a) The electronic band structures along armchair (left panel) and zigzag (right panel) edges. The solid and dashed curves represent the edge state dispersions with and without in-plane magnetic field. (b) The relative energies of Dirac points $\Delta E_{\mathrm{DP}} = E_{\mathrm{DP}}(\theta) - E_{\mathrm{DP}}(\pi/2)$ (the black dashed curve) and the edge state gap (the blue curve) as a function of the edge cut directions with the magnetic field along the x direction (black arrow). (c) The gap at the zigzag (blue curves) and armchair edges (red curves) as a function of the in-plane magnetic field directions with different amplitudes. (d) The wave function plot with its eigenvalue closest to zero. The black arrow indicates the magnetic field direction.

weakly break the mirror symmetries, such as the Rashba SOC, weak disorders, and the rotation of the various Majorana patterns by a small angle. Next, we discuss the possible experimental realization.

Anisotropic edge states gap.—To demonstrate the experimental accessibility of our proposal, we start from the Zhang-Li-Wu (ZLW) model [61] for a single layer bismuth grown on SiC substrate, which has been experimentally reported to have large quantum spin Hall gap around 0.435 eV [62] and one-dimensional edge states [63]. However our results are also applied to other 2DTI such as the Kane-Mele model for graphene [64,65] and the Liu-Jiang-Yao model [66] for silicene with p_z. The ZLW model with $\{p_x, p_y\}$ orbitals forming the 2DTI bands takes the form [61,67]

$$\begin{aligned} H = & \sum_{\langle ij\rangle} t_\sigma^{(1)} p_{i,\boldsymbol{a}_{ij}}^\dagger p_{j,\boldsymbol{a}_{ij}} + t_\pi^{(1)} p_{i,\boldsymbol{a}_{ij}}'^\dagger p_{j,\boldsymbol{a}_{ij}}' \\ & + \sum_{\langle\langle ij\rangle\rangle} t_\sigma^{(2)} p_{i,\boldsymbol{b}_{ij}}^\dagger p_{j,\boldsymbol{b}_{ij}} + t_\pi^{(2)} p_{i,\boldsymbol{b}_{ij}}'^\dagger p_{j,\boldsymbol{b}_{ij}}' \\ & - \sum_{i,s} i\lambda_{so} p_{i,x}^\dagger s_z p_{i,y} + \mathrm{H.c.} \end{aligned} \tag{1}$$

where $t_{\sigma(\pi)}^1$, $t_{\sigma(\pi)}^2$, λ_{so} are the usual $\sigma(\pi)$ bond strengths between nearest neighbor sites, next-nearest neighbor sites, the intrinsic SOC strengths, respectively, $p_{i,\boldsymbol{a}_{ij}}$ ($p_{i,\boldsymbol{b}_{ij}}$) and $p'_{i,\boldsymbol{a}_{ij}}$ ($p'_{i,\boldsymbol{b}_{ij}}$) are the projections of $\{p_x, p_y\}$ orbitals parallel and perpendicular to the bond direction $\boldsymbol{a}_{ij}$ ($\boldsymbol{b}_{ij}$) for the first (second) nearest hopping, respectively [68], $s_z = \pm$ refers to spin-up and spin-down, $\langle\ldots\rangle$ and $\langle\langle\ldots\rangle\rangle$ are the summations for the nearest and next-nearest neighbors, respectively. In the rest of this Letter, we take $t_\sigma^{(1)} = 2$ eV, $t_\pi^{(1)} = -0.21$ eV, $t_\sigma^{(2)} = -0.15$ eV, $t_\pi^{(2)} = -0.05$ eV, $\lambda_{\mathrm{so}} = 0.435$ eV according to Ref. [62]. The system has time-reversal symmetry protected by gapless helical edge states [black dashed curves in Fig. 2(a)]. As the second nearest neighbor hopping breaks the "particle-hole" symmetry (the symmetric band dispersion between conduction and valence bands), the energies of Dirac points, E_{DP}, at armchair and zigzag edges are different, which is normally the case for the real situation [62]. The E_{DP} shows a C_3 rotational symmetry [black dashed curves in Fig. 2(b)].

We now consider applying a uniform in-plane magnetic field into the system. The Zeeman splitting under an in-plane magnetic field in both bismuthene and silicene systems takes the form $Ms_\parallel$ [68], which in general is expected to open a gap, referred to as a Zeeman gap, for the helical edge states along any edge directions because it breaks time-reversal symmetry and couples the states with opposite spin along the z direction. Here $s_\parallel$ implies the spin along the in-plane magnetic field direction. We find that the helical edge states at the zigzag edge acquires a finite gap Δ_z, with the amplitude approximately equal to the Zeeman splitting energy. On the other hand, the Zeeman gap at armchair edge, Δ_a, is very small, the ratio $\Delta_a/M < 10^{-2}$ which are similar with the previous study in either silicene [74] or bismuthene [75] without breaking "particle-hole" symmetry. Remarkably, we find that the quasimetallic state at armchair edge is also robust against breaking the "particle-hole" symmetry. The Zeeman gap and its gap

center are plotted in terms of the edge direction given the magnetic field along the x direction and show high anisotropy with a periodicity of $\pi/3$ [Fig. 2(b)], which reflects the C_3 symmetry of the Hamiltonian [Eq. (1)]. We further explore whether the magnetic field direction affects our results. In Fig. 2(c), we plot the Zeeman gaps of the zigzag (armchair) edge in the blue (red) curves as a function of the magnetic field direction. For all directions, the Zeeman gap at the zigzag edge takes the value around the Zeeman splitting energy while the armchair edge remains almost gapless. Thus when the zigzag edges are insulating, the armchair edges always behave like a one-dimensional (1D) single channel metallic wire [Fig. 2(d)] regardless of the in-plane magnetic field direction.

We further apply an uniform conventional s-wave and spin-singlet superconducting gap function with gap amplitude Δ_{sc} into system. For simplicity, we take μ to be the Zeeman gap center at zigzag edges. But our results generally remain valid for varying μ [68]. In Fig. 3(a), we plot the edge state gaps, Δ_a and Δ_z, as a function of the superconducting gap Δ_{sc} with a fixed M. For the armchair edge, the previous metallic edge states are gapped with $\Delta_a \approx \Delta_{sc}$. For the zigzag edge, the edge states undergo a phase transition, from Zeeman dominated gap states to superconductivity dominated gap states [Fig. 3(a)], as the gap closes and reopens. In Figs. 3(b) and 3(c), we plot the gap of the edge states at the armchair edge and zigzag edge, respectively, as a function of superconducting gap amplitude Δ_{sc} and the Zeeman splitting energy M. For the armchair edge, the gap remains finite as long as Δ_{sc} is finite, and thus the gap Δ_a is dominated by superconductivity regardless of the strength of magnetic field. For the zigzag edge, the gap is closed approximately at $\Delta_{sc} = M$ and reopened. As the superconducting gap function and the in-plane Zeeman term commute, the edge states at Dirac point are the eigenfunction of the superconducting matrix τ_x. There are two negative energy edge states with eigenvalues $\nu_1^z = \nu_2^z = -1$ for $\Delta_{sc} - M > 0$ and $\nu_1^z = -\nu_2^z = -1$ for $\Delta_{sc} - M < 0$. Meanwhile, the gap of the armchair edge states is always dominated by the superconductivity so that the two negative energy edge states always have eigenvalues $\nu_1^a = \nu_2^a = -1$. We thus can define a topological invariant $\nu = \prod_{i=1}^{2} \nu_i^a \nu_i^z$ [68]. For $\nu = -1$, the armchair and zigzag edges are in two topologically different phases, which implies that a single MZM exists at the corner between these two types of edges. When the chemical potential varies from the Zeeman gap center at the zigzag edge, the MZM is still robust as long as the edge gap is not closed [68]. In the Supplemental Material [68], we also study the Wannier bands [27] of edge states as a function of M/Δ_{sc}, which has a sudden jump at the topological phase transition of ν. We found that the celebrated Kitaev spinless p-wave model also has similar behavior by calculating the logarithm of its Wilson loop. These results clearly reflect the topological origin of our proposal. We further plot the

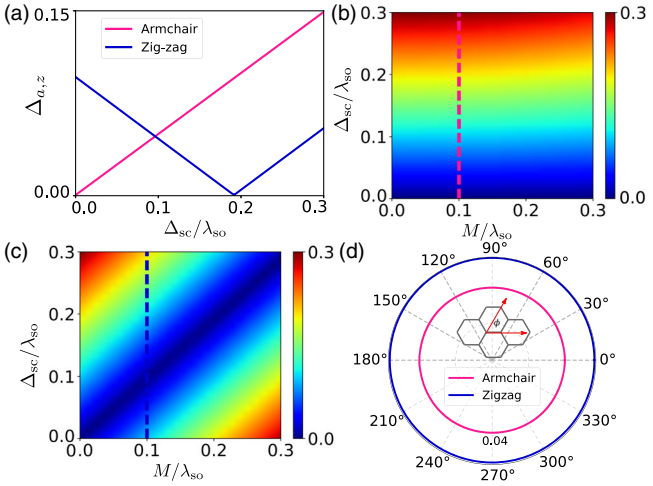

FIG. 3. (a) The gaps for the zigzag and armchair edges as a function of the superconducting gap Δ_{sc} with the in-plane magnetic field, $M/\lambda_{so} = 0.1$, along the x direction. (b) and (c) The color plot of the gap at the armchair and zigzag edges, respectively, under the in-plane magnetic field and superconducting amplitudes. (d) The edge state gap as a function of the in-plane magnetic field direction with $M/\lambda_{so} = 0.1$ and $\Delta_{sc}/\lambda_{so} = 0.04$. For this plot, we choose the armchair and zigzag edges along x and y directions, respectively.

gaps at two edges as a function of the magnetic field direction and found that the gap amplitudes on two edges are independent of the magnetic field directions [Fig. 3(d)]. Thus our results are insensitive to the in-plane magnetic field direction.

Majorana patterns.—As discussed above, our theory has indicated the existence of MZMs at the corner between the armchair and zigzag edges. Below, we will consider the realization of these corners in the sample patterns of polygons, particularly triangle patterns. As the whole system only allows for an even number of MZMs, the triangle can only support up to two MZMs at the two of its three corners. For the honeycomb lattice, the angles between the armchair and zigzag edges can take the values $\pi/6$, $\pi/2$, and $5\pi/6$, while those between the same type of edge are $\pi/3$ and $2\pi/3$. We hope that three edges of the triangle are either armchair or zigzag boundary and identify two triangle configurations for this condition. One is an obtuse isosceles triangle with the obtuse interior angle of $2\pi/3$ [Fig. 1(a)] and the other is a right triangle with one acute interior angle of $\pi/6$ [Fig. 1(a)]. Due to the C_3 rotational symmetry of the honeycomb lattice, there are six orientations for each triangle configuration as shown in Figs. 1(a) and 1(b). We then calculate the eigenvalues of the system with these two triangle configurations and found that in the range $0 < \Delta_{sc} < M$, each of them support two zero modes, shown in the insets of the Figs. 4(a) and 4(b). The density plots of these two zero modes in the two triangular patterns [Figs. 4(a) and 4(b)] show that they separately locate at two of the three corners with the interior

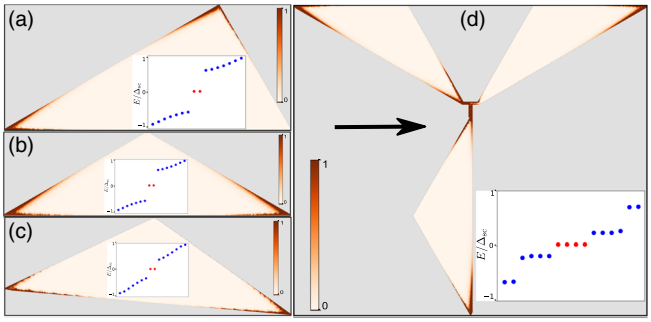

FIG. 4. (a) and (b) The density plot of MZMs in Majorana isosceles and right triangles. (c) Majorana triangles with the edges have a 5° deviation from the armchair and zigzag edges, respectively. (d) Y junction made from three Majorana isosceles triangles. The black arrow indicate the in-plane magnetic field direction. The insets plot the energies of the eigenstates.

angles of $\pi/6$ for the isosceles triangle and with the interior angles of $\pi/6$ and $\pi/2$ for the right triangle. We thus dub these two triangle configurations as Majorana triangles. As these Majorana triangles host only two MZMs, they are topologically equivalent to the Majorana nanowire [1–4]. Importantly, because the applied in-plane magnetic field direction will not affect the gaps at armchair and zigzag edges, all the Majorana triangles on these six orientations can have MZMs under the same in-plane magnetic field. Note that the local single MZM is topologically stable and does not require additional symmetry, we rotate the Majorana triangle by 5° and the spatially separated MZMs are still stable even there is no symmetries at each edge. All these features have the advantage of realizing more complex Majorana structures. In Fig. 4(d), we construct the Y junction, which is proposed to realize Majorana braiding [76–80]. The density plot and the eigenvalue calculations show that there are four MZMs in these constructions that are well separated from each other. The additional two modes with the eigenenergies are closer to zero than the other excited states are from the coupled Majorana bound states at the center of the Y junction. The color bar with the logarithmic scale shows that they are well separated from the four MZMs in the energy space. Importantly, it should be noted that this Y junction is realized under the uniform in-plane magnetic field. Note that the MZM at each corner is protected by topology; the slight symmetry broken by Rashba SOC does not affect the robustness of the MZM at all.

Magnetic gap at the armchair edge.—We here analyze the gap anisotropy based on the edge theory. At the Dirac point with $k_x = 0$, which only contains σ_x and σ_z [68], the edge states for the semi-infinite system with $y \in (-\infty, 0)$ generally take the form

$$\Psi_{n=1,2}(y) = N \sin(\alpha y) e^{\beta y} \chi_{n=1,2},$$
$$\chi_1 = |\uparrow\rangle \otimes |\sigma_y = 1\rangle, \qquad \chi_2 = |\downarrow\rangle \otimes |\sigma_y = -1\rangle, \quad (2)$$

with α and β being the wave vector and the decay rate of the edge states. Here χ_1 and χ_2 are time-reversal partners. Noted that this form of the helical edge state is not by accident, but enforced by the mirror symmetry. This is because the nearest neighbor hopping term conserves spin and thus can be only proportional to $\sigma_x s_0$ and $\sigma_y s_0$. Meanwhile, along the armchair edge, it also respects the mirror-x symmetry ($\hat{M}_x = i s_x \sigma_x$), so that the nearest hopping term for the zigzag edge can be only proportional to $\sigma_x s_0$ [68]. In addiction, the SOC term is always proportional to $\sigma_z s_z$. Thus the helical edge states at $k_x = 0$ must take the form of Eq. (2) [68]. We then project the 1D Hamiltonian along y direction with finite k_x [68] into the two-dimensional basis $\Psi_n e^{ik_x x}$ and get the effective edge state Hamiltonian [68]

$$H_{\text{edge}} = -\frac{\sqrt{3}}{4} t_m^{(1)} k_x \tilde{s}_z - \frac{3}{2} t_p^{(2)}, \quad (3)$$

with $\tilde{s}$ acting on the $(\Psi_1, \Psi_2)^{\mathrm{T}}$ basis. Note that $\langle \Psi_i | M \sigma_0 s_\parallel | \Psi_j \rangle = 0$ for all $i = 1, 2$ and $j = 1, 2$, the in-plane magnetic Zeeman term completely vanishes in the effective edge Hamiltonian. We found that for the edge states in Eq. (2), only the antiferromagnetic term such as $\sigma_z s_\parallel$ can directly open a gap while the ferromagnetic term $\sigma_0 s_\parallel$ can not. The in-plane magnetic field lead to ferromagneticlike Zeeman splitting [68] and thus cannot open a gap at the armchair edge. On the other hand, the antiferromagnetic term can come from the magnetic field fluctuation. Note that this analysis holds for all the armchair edges with the in-plane ferromagnetic or antiferromagnetic terms in all directions. Although the antiferromagnetic term can open a gap in both armchair and zigzag edges, the Majorana corner states still remain robust because when the chemical potential is inside the zigzag edge state gap, it is away from the E_{DP} at armchair edge so that the armchair edge are always superconducting. Thus, the Majorana corner states remain even in the presence of the in-plane antiferromagnetic term [68], and thus it is robust against the inhomogeneity of the magnetic field. We also find that the weak spin-independent disorder will not affect the wave function forms of χ_1 and χ_2. Thus our results remain valid against weak spin-independent disorder [68].

Conclusion and discussion.—In conclusion, we propose to realize the second order TSC in the D class and the corner MZMs based on 2DTI under a uniform in-plane magnetic field and in proximity to s-wave superconductors. Our scheme is shown with the realistic bismuthene model but also valid for other 2DTI model such as silicene, germanene, and stanene, and may have the advantage in constructing Majorana networks. For the monolayer $NbSe_2$ superconductor, the superconducting gap is about 0.5 meV and the in-plane critical field can be as large as 27T [81]. For the in-plane magnetic field of 10T with the g factor $g = 2$, the Zeeman splitting energy is about 1.2 meV. As the

single MZM is topologically robust against the local perturbation, we show that our results hold even in the presence of various perturbations. So our proposal maybe realized under the reasonable material parameters.

We would like to thank Yugui Yao, Cheng-Cheng Liu, Jinhua Gao, Aiyun Luo, and Xiong-Jun Liu for fruitful discussions. X. L. acknowledges the support of the Ministry of Science and Technology of China (Grant No. 2016YFA0401003) and the National Natural Science Foundation of China (Grant No. 11674114). G. X. acknowledges the support of the Ministry of Science and Technology of China (Grant No. 2018YFA0307000), and the National Natural Science Foundation of China (Grant No. 11874022). C.-X. L. acknowledges the support of the Office of Naval Research (Grant No. N00014-18-1-2793), the U.S. Department of Energy (Grant No. DESC0019064) and Kaufman New Initiative research grant (Grant No. KA2018-98553) of the Pittsburgh Foundation.

*phyliuxin@hust.edu.cn

[1] A. Y. Kitaev, Phys. Usp. **44**, 131 (2001).
[2] J. D. Sau, R. M. Lutchyn, S. Tewari, and S. Das Sarma, Phys. Rev. Lett. **104**, 040502 (2010).
[3] R. M. Lutchyn, J. D. Sau, and S. Das Sarma, Phys. Rev. Lett. **105**, 077001 (2010).
[4] Y. Oreg, G. Refael, and F. von Oppen, Phys. Rev. Lett. **105**, 177002 (2010).
[5] V. Mourik, K. Zuo, S. M. Frolov, S. R. Plissard, E. P. A. M. Bakkers, and L. P. Kouwenhoven, Science **336**, 1003 (2012).
[6] M. T. Deng, C. L. Yu, G. Y. Huang, M. Larsson, P. Caroff, and H. Q. Xu, Nano Lett. **12**, 6414 (2012).
[7] L. P. Rokhinson, X. Liu, and J. K. Furdyna, Nat. Phys. **8**, 795 (2012).
[8] A. Das, Y. Ronen, Y. Most, Y. Oreg, M. Heiblum, and H. Shtrikman, Nat. Phys. **8**, 887 (2012).
[9] M.-X. Wang, C. Liu, J.-P. Xu, F. Yang, L. Miao, M.-Y. Yao, C. L. Gao, C. Shen, X. Ma, X. Chen, Z.-A. Xu, Y. Liu, S.-C. Zhang, D. Qian, J.-F. Jia, and Q.-K. Xue, Science **336**, 52 (2012).
[10] H. O. H. Churchill, V. Fatemi, K. Grove-Rasmussen, M. T. Deng, P. Caroff, H. Q. Xu, and C. M. Marcus, Phys. Rev. B **87**, 241401(R) (2013).
[11] J.-P. Xu, C. Liu, M.-X. Wang, J. Ge, Z.-L. Liu, X. Yang, Y. Chen, Y. Liu, Z.-A. Xu, C.-L. Gao, D. Qian, F.-C. Zhang, and J.-F. Jia, Phys. Rev. Lett. **112**, 217001 (2014).
[12] S. Nadj-Perge, I. K. Drozdov, J. Li, H. Chen, S. Jeon, J. Seo, A. H. MacDonald, B. A. Bernevig, and A. Yazdani, Science **346**, 602 (2014).
[13] W. Chang, S. M. Albrecht, T. S. Jespersen, F. Kuemmeth, P. Krogstrup, J. Nygrd, and C. M. Marcus, Nat. Nanotechnol. **10**, 232 (2015).
[14] H.-H. Sun, K.-W. Zhang, L.-H. Hu, C. Li, G.-Y. Wang, H.-Y. Ma, Z.-A. Xu, C.-L. Gao, D.-D. Guan, Y.-Y. Li, C. Liu, D. Qian, Y. Zhou, L. Fu, S.-C. Li, F.-C. Zhang, and J.-F. Jia, Phys. Rev. Lett. **116**, 257003 (2016).
[15] S. M. Albrecht, A. P. Higginbotham, M. Madsen, F. Kuemmeth, T. S. Jespersen, J. Nygrd, P. Krogstrup, and C. M. Marcus, Nature (London) **531**, 206 (2016).
[16] J. Wiedenmann, E. Bocquillon, R. S. Deacon, S. Hartinger, O. Herrmann, T. M. Klapwijk, L. Maier, C. Ames, C. Brne, C. Gould, A. Oiwa, K. Ishibashi, S. Tarucha, H. Buhmann, and L. W. Molenkamp, Nat. Commun. **7**, 10303 (2016).
[17] E. Bocquillon, R. S. Deacon, J. Wiedenmann, P. Leubner, T. M. Klapwijk, C. Brne, K. Ishibashi, H. Buhmann, and L. W. Molenkamp, Nat. Nanotechnol. **12**, 137 (2017).
[18] K. Zhang, J. Zeng, Y. Ren, and Z. Qiao, Phys. Rev. B **96**, 085117 (2017).
[19] H. Zhang *et al.*, Nature (London) **556**, 74 (2018).
[20] P. Zhang, K. Yaji, T. Hashimoto, Y. Ota, T. Kondo, K. Okazaki, Z. Wang, J. Wen, G. D. Gu, H. Ding, and S. Shin, Science **360**, 182 (2018).
[21] D. Wang, L. Kong, P. Fan, H. Chen, S. Zhu, W. Liu, L. Cao, Y. Sun, S. Du, J. Schneeloch, R. Zhong, G. Gu, L. Fu, H. Ding, and H.-J. Gao, Science **362**, 333 (2018).
[22] D. A. Ivanov, Phys. Rev. Lett. **86**, 268 (2001).
[23] C. Nayak, S. H. Simon, A. Stern, M. Freedman, and S. Das Sarma, Rev. Mod. Phys. **80**, 1083 (2008).
[24] D. Laroche, D. Bouman, D. J. van Woerkom, A. Proutski, C. Murthy, D. I. Pikulin, C. Nayak, R. J. J. van Gulik, J. Nygrd, P. Krogstrup, L. P. Kouwenhoven, and A. Geresdi, Nat. Commun. **10**, 245 (2019).
[25] R. S. Deacon, J. Wiedenmann, E. Bocquillon, F. Domínguez, T. M. Klapwijk, P. Leubner, C. Brüne, E. M. Hankiewicz, S. Tarucha, K. Ishibashi, H. Buhmann, and L. W. Molenkamp, Phys. Rev. X **7**, 021011 (2017).
[26] F. Zhang, C. L. Kane, and E. J. Mele, Phys. Rev. Lett. **110**, 046404 (2013).
[27] W. A. Benalcazar, B. A. Bernevig, and T. L. Hughes, Science **357**, 61 (2017).
[28] C. Fang and L. Fu, arXiv:1709.01929.
[29] L. Peng, Y. Yuan, G. Li, X. Yang, J.-J. Xian, C.-J. Yi, Y.-G. Shi, and Y.-S. Fu, Nat. Commun. **8**, 659 (2017).
[30] W. A. Benalcazar, B. A. Bernevig, and T. L. Hughes, Phys. Rev. B **96**, 245115 (2017).
[31] J. Langbehn, Y. Peng, L. Trifunovic, F. von Oppen, and P. W. Brouwer, Phys. Rev. Lett. **119**, 246401 (2017).
[32] Z. Song, Z. Fang, and C. Fang, Phys. Rev. Lett. **119**, 246402 (2017).
[33] L. Li, H. H. Yap, M. A. N. Araújo, and J. Gong, Phys. Rev. B **96**, 235424 (2017).
[34] M. Ezawa, Phys. Rev. Lett. **120**, 026801 (2018).
[35] H. Shapourian, Y. Wang, and S. Ryu, Phys. Rev. B **97**, 094508 (2018).
[36] M. Serra-Garcia, V. Peri, R. Ssstrunk, O. R. Bilal, T. Larsen, L. G. Villanueva, and S. D. Huber, Nature (London) **555**, 342 (2018).
[37] C. W. Peterson, W. A. Benalcazar, T. L. Hughes, and G. Bahl, Nature (London) **555**, 346 (2018).
[38] X. Zhu, Phys. Rev. B **97**, 205134 (2018).
[39] M. Ezawa, Sci. Rep. **9**, 5286 (2019).
[40] M. Geier, L. Trifunovic, M. Hoskam, and P. W. Brouwer, Phys. Rev. B **97**, 205135 (2018).
[41] E. Khalaf, Phys. Rev. B **97**, 205136 (2018).
[42] F. Schindler, A. M. Cook, M. G. Vergniory, Z. Wang, S. S. P. Parkin, B. A. Bernevig, and T. Neupert, Sci. Adv. **4**, 0346 (2018) .

[43] M. Ezawa, Phys. Rev. B **97**, 241402(R) (2018).
[44] T. Liu, J. J. He, and F. Nori, Phys. Rev. B **98**, 245413 (2018).
[45] Z. Wang, B. J. Wieder, J. Li, B. Yan, and B. A. Bernevig, arXiv:1806.11116.
[46] B. J. Wieder, B. Bradlyn, Z. Wang, J. Cano, Y. Kim, H.-S. D. Kim, A. M. Rappe, C. L. Kane, and B. A. Bernevig, Science **361**, 246 (2018).
[47] F. Schindler, Z. Wang, M. G. Vergniory, A. M. Cook, A. Murani, S. Sengupta, A. Y. Kasumov, R. Deblock, S. Jeon, I. Drozdov, H. Bouchiat, S. Guron, A. Yazdani, B. A. Bernevig, and T. Neupert, Nat. Phys. **14**, 918 (2018).
[48] M. Ezawa, Phys. Rev. B **98**, 045125 (2018).
[49] M. Ezawa, Phys. Rev. B **97**, 155305 (2018).
[50] Q. Wang, C.-C. Liu, Y.-M. Lu, and F. Zhang, Phys. Rev. Lett. **121**, 186801 (2018).
[51] V. Dwivedi, C. Hickey, T. Eschmann, and S. Trebst, Phys. Rev. B **98**, 054432 (2018).
[52] Z. Yan, F. Song, and Z. Wang, Phys. Rev. Lett. **121**, 096803 (2018).
[53] N. Bultinck, B. A. Bernevig, and M. P. Zaletel, Phys. Rev. B **99**, 125149 (2019).
[54] S. Imhof, C. Berger, F. Bayer, J. Brehm, L. W. Molenkamp, T. Kiessling, F. Schindler, C. H. Lee, M. Greiter, T. Neupert, and R. Thomale, Nat. Phys. **14**, 925 (2018).
[55] Y. You, D. Litinski, and F. von Oppen, Phys. Rev. B **100**, 054513 (2019).
[56] Y. Wang, M. Lin, and T. L. Hughes, Phys. Rev. B **98**, 165144 (2018).
[57] B. Huang and W. V. Liu, arXiv:1811.00555.
[58] C.-H. Hsu, P. Stano, J. Klinovaja, and D. Loss, Phys. Rev. Lett. **121**, 196801 (2018).
[59] R. Queiroz and A. Stern, Phys. Rev. Lett. **123**, 036802 (2019).
[60] R.-X. Zhang, W. S. Cole, and S. Das Sarma, Phys. Rev. Lett. **122**, 187001 (2019).
[61] G.-F. Zhang, Y. Li, and C. Wu, Phys. Rev. B **90**, 075114 (2014).
[62] F. Reis, G. Li, L. Dudy, M. Bauernfeind, S. Glass, W. Hanke, R. Thomale, J. Schäfer, and R. Claessen, Science **357**, 287 (2017).
[63] R. Stühler, F. Reis, T. Müller, T. Helbig, T. Schwemmer, R. Thomale, J. Schäfer, and R. Claessen, arXiv:1901.06170.
[64] C. L. Kane and E. J. Mele, Phys. Rev. Lett. **95**, 226801 (2005).
[65] C. L. Kane and E. J. Mele, Phys. Rev. Lett. **95**, 146802 (2005).
[66] C.-C. Liu, W. Feng, and Y. Yao, Phys. Rev. Lett. **107**, 076802 (2011).
[67] G. Li, W. Hanke, E. M. Hankiewicz, F. Reis, J. Schäfer, R. Claessen, C. Wu, and R. Thomale, Phys. Rev. B **98**, 165146 (2018).
[68] See Supplemental Material at http://link.aps.org/supplemental/10.1103/PhysRevLett.123.156801 for the following: I. A The Hamiltonian of Bismuthene on SiC. I .B The in-plane antiferromagnetic field effect on the Majorana corner states. II .A The second-order topological superconductors and Majorana patterns in two-dimension silicene germanium and stanene. II. B The numerical calculations of the Rashba and weak disorder effect on the gap of the edge states at armchair edge with in-plane magnetic field. II. C The finite chemical potential effect on the Majorana corner states. III. A The discussion of Z2 topological invariant. III. B Wannier band calculations, which includes Refs. [69–73].
[69] S. Cahangirov, M. Topsakal, E. Aktürk, H. Şahin, and S. Ciraci, Phys. Rev. Lett. **102**, 236804 (2009).
[70] C.-C. Liu, H. Jiang, and Y. Yao, Phys. Rev. B **84**, 195430 (2011).
[71] N. D. Drummond, V. Zólyomi, and V. I. Fal'ko, Phys. Rev. B **85**, 075423 (2012).
[72] M. Ezawa, Phys. Rev. Lett. **109**, 055502 (2012).
[73] M. Ezawa, Phys. Rev. B **87**, 155415 (2013).
[74] D. Kuzmanovski, J. Linder, and A. Black-Schaffer, Phys. Rev. B **94**, 180505(R) (2016).
[75] F. Dominguez, B. Scharf, G. Li, J. Schäfer, R. Claessen, W. Hanke, R. Thomale, and E. M. Hankiewicz, Phys. Rev. B **98**, 161407(R) (2018).
[76] D. J. Clarke, J. D. Sau, and S. Tewari, Phys. Rev. B **84**, 035120 (2011).
[77] J. D. Sau, D. J. Clarke, and S. Tewari, Phys. Rev. B **84**, 094505 (2011).
[78] B. van Heck, A. R. Akhmerov, F. Hassler, M. Burrello, and C. W. J. Beenakker, New J. Phys. **14**, 035019 (2012).
[79] T. Hyart, B. van Heck, I. C. Fulga, M. Burrello, A. R. Akhmerov, and C. W. J. Beenakker, Phys. Rev. B **88**, 035121 (2013).
[80] L.-H. Wu, Q.-F. Liang, and X. Hu, Sci. Technol. Adv. Mater. **15**, 064402 (2014).
[81] X. Xi, Z. Wang, W. Zhao, J.-H. Park, K. T. Law, H. Berger, L. Forr, J. Shan, and K. F. Mak, Nat. Phys. **12**, 139 (2016).